

# Abundances of ethylene oxide and acetaldehyde in hot molecular cloud cores

A. Nummelin<sup>1</sup>, J.E. Dickens<sup>2</sup>, P. Bergman<sup>1</sup>, Å. Hjalmarsen<sup>1</sup>, W. M. Irvine<sup>2</sup>, M. Ikeda<sup>3</sup>, and M. Ohishi<sup>4</sup>

<sup>1</sup> Onsala Space Observatory, S-439 92 Onsala, Sweden

<sup>2</sup> FCRAO, 619 Lederle GRC, University of Massachusetts, Amherst, MA 01003, USA

<sup>3</sup> Nobeyama Radio Observatory, Nobeyama, Minamimaki, Minamisaku, Nagano 384-13, Japan

<sup>4</sup> National Astronomical Observatory of Japan, 2-21-1, Osawa, Mitaka, Tokyo 181-8588, Japan

Received 28 May 1998 / Accepted 12 June 1998

**Abstract.** We have searched for millimetre-wave line emission from ethylene oxide (c-C<sub>2</sub>H<sub>4</sub>O) and its structural isomer acetaldehyde (CH<sub>3</sub>CHO) in 11 molecular clouds using SEST. Ethylene oxide and acetaldehyde were detected through multiple lines in the hot cores NGC 6334F, G327.3–0.6, G31.41+0.31, and G34.3+0.2. Acetaldehyde was also detected towards G10.47+0.03, G322.2+0.6, and Orion 3'N, and one ethylene oxide line was tentatively detected in G10.47+0.03. Column densities and rotational excitation temperatures were derived using a procedure which fits the observed line intensities by finding the minimum  $\chi^2$ -value. The resulting rotational excitation temperatures of ethylene oxide and acetaldehyde are in the range 16–38 K, indicating that these species are excited in the outer, cooler parts of the hot cores or that the excitation is significantly subthermal. For an assumed source size of 20'', the deduced column densities are  $(0.6–1)\times 10^{14}$  cm<sup>-2</sup> for ethylene oxide and  $(2–5)\times 10^{14}$  cm<sup>-2</sup> for acetaldehyde. The fractional abundances with respect to H<sub>2</sub> are  $X[\text{c-C}_2\text{H}_4\text{O}]=(2–6)\times 10^{-10}$ , and  $X[\text{CH}_3\text{CHO}]= (0.8–3)\times 10^{-9}$ . The ratio  $X[\text{CH}_3\text{CHO}]/X[\text{c-C}_2\text{H}_4\text{O}]$  varies between 2.6 (NGC 6334F) and 8.5 (G327.3–0.6). We also detected and analysed multiple transitions of CH<sub>3</sub>OH, CH<sub>3</sub>OCH<sub>3</sub>, C<sub>2</sub>H<sub>5</sub>OH, and HCOOH. The chemical, and possibly evolutionary, states of NGC 6334F, G327.3–0.6, G31.41+0.31, and G34.3+0.2 seem to be very similar.

**Key words:** ISM: molecules – ISM: abundances – ISM: H II-regions – radio lines: ISM

## 1. Introduction

Ethylene oxide (c-C<sub>2</sub>H<sub>4</sub>O) was recently detected astronomically for the first time towards Sgr B2(N) (Dickens et al. 1997). It is the third molecule with a cyclic structure to be found in the interstellar medium and is the first such molecule to contain oxygen. Ethylene oxide is a higher-energy structural isomer of acetaldehyde (CH<sub>3</sub>CHO), a familiar interstellar molecule detected

towards both giant molecular clouds (e.g. Gilmore et al. 1976) and dark clouds (Matthews, Friberg, & Irvine 1985). There is also a third isomeric form, vinyl alcohol (CH<sub>2</sub>CHOH), which is intermediate in energy but, as yet, undetected astronomically although searched for (Irvine et al. 1989). Both acetaldehyde and vinyl alcohol have chain structures.

Due to its two pairs of interchangeable identical hydrogen nuclei ethylene oxide has two different symmetry states which can be denoted *ortho* (symmetric) and *para* (antisymmetric). These states correspond to energy levels with quantum numbers  $K_a K_c$  *ee/oo* (*ortho*) and *eo/oe* (*para*) and have spin weights which are equal to 10 and 6, respectively. The rotational spectrum of ethylene oxide is purely *b*-type ( $\mu_b=1.88$  D). Acetaldehyde has both *a*- and *b*-type transitions ( $\mu_a=2.423$  D,  $\mu_b=1.266$  D) and the internal rotation of the methyl group gives rise to two non-interacting torsional substates, denoted *A* and *E*, the ground state energies of which are separated by 0.1 K.

Because of the unusual structure of ethylene oxide relative to most known interstellar molecules, it is interesting to investigate the distribution and abundance of such a molecule in the interstellar medium to find out how the distribution and excitation of this molecule compare to other molecules, e.g., acetaldehyde. Since structural isomers typically share some production and destruction pathways the relative abundance of two such isomers could provide important constraints on astrochemical models. We have therefore searched for emission from the ethylene oxide-acetaldehyde isomeric pair in a number of molecular clouds. The majority of the targeted sources are warm and dense condensations of molecular gas, in most cases found inside massive star-forming regions. Some of these sources, often called “hot cores” after the original such source in Orion, have been shown to be have very rich gas-phase chemistry (van Dishoeck & Blake 1998).

The organisation of this paper is as follows. In Sects. 2 and 3 we describe the details of the observations, data reduction, and a simple  $\chi^2$ -minimisation method for finding the column density and rotational temperature that best reproduces the observed line intensities. In Sect. 4 we present the observational data for each source. Sample spectra are shown together with rotation diagrams for ethylene oxide and acetaldehyde, and tabulations

of derived rotational excitation temperatures, column densities, and abundances. In Sect. 5 we compare the deduced molecular abundances with chemical models, and finally, in Sect. 6, we summarise our main conclusions. In Appendix A we list the partition functions and statistical weights for  $c\text{-C}_2\text{H}_4\text{O}$  and  $\text{CH}_3\text{CHO}$ .

## 2. Observations and data reduction

The observations were performed using the 15-meter Swedish-ESO Submillimetre Telescope<sup>1</sup> (SEST) at La Silla, Chile, during October 1997. The 1.3 mm and 3 mm data were obtained simultaneously using the IRAM-built 230/115 GHz SIS receiver, with both channels tuned to single-sideband (SSB) operation. Hence, no post-processing of the data to separate the sideband response was necessary. The system temperatures were 200–600 K, in the 1.3 mm band and 180–250 K in the 3 mm band. The data were chopper-wheel calibrated (Kutner & Ulich 1981) and the raw data were obtained as atmosphere-corrected antenna temperature ( $T_A^*$ ). Before analysis, this was converted to main-beam brightness temperature ( $T_{\text{mb}}$ ) through  $T_{\text{mb}} = T_A^*/\eta_{\text{mb}}$  where  $\eta_{\text{mb}}$ , the main-beam efficiency as defined by Mangum (1993), is 0.6 for the 230 GHz band, and 0.75 for the 115 GHz band.

The telescope pointing and subreflector focusing were checked regularly on the SiO masers in VX Sgr and AH Sco. We estimate the uncertainty in antenna temperature due to pointing and calibration errors to be 20%.

The 3 mm receiver channel was connected to a narrow-band (86 MHz) Acousto-Optical Spectrometer (AOS) with a nominal channel separation of 0.043 MHz, and in the 1.3 mm band a wide-band (1 GHz) AOS with 0.7 MHz per channel was used. Because of the channel correlation, the actual frequency resolutions obtained in the two spectrometers are 0.080 MHz ( $0.25 \text{ km s}^{-1}$ ) and 1.4 MHz ( $1.8 \text{ km s}^{-1}$ ).

All data were obtained in dual beam-switch mode with an azimuthal beam separation of  $11.6'$ , and the baselines are very flat in all spectra. Hence, only the continuum levels were subtracted from the spectra. The peak main-beam brightness temperature, full linewidth at half maximum (FWHM), and centre frequency, were estimated by fitting Gaussians to the observed spectral lines.

In order to compare intensities of lines in the 1.3 mm and 3 mm bands, we applied a correction for the beam-filling to the intensity of each observed line. Assuming that the source brightness distribution and the antenna response are both Gaussian this correction factor,  $\eta_s$ , can be written as

$$\eta_s = \frac{\theta_s^2}{\theta_{\text{mb}}^2 + \theta_s^2}$$

where  $\theta_s$  is the source size and  $\theta_{\text{mb}}$  is the (frequency dependent) beam-size of the antenna. In our analysis we have adopted a source size equal to the size of the smallest beam,  $20''$  (at

<sup>1</sup> The Swedish-ESO Submillimetre Telescope is operated jointly by ESO and the Swedish National Facility for Radio Astronomy, Onsala Space Observatory, at Chalmers University of Technology.

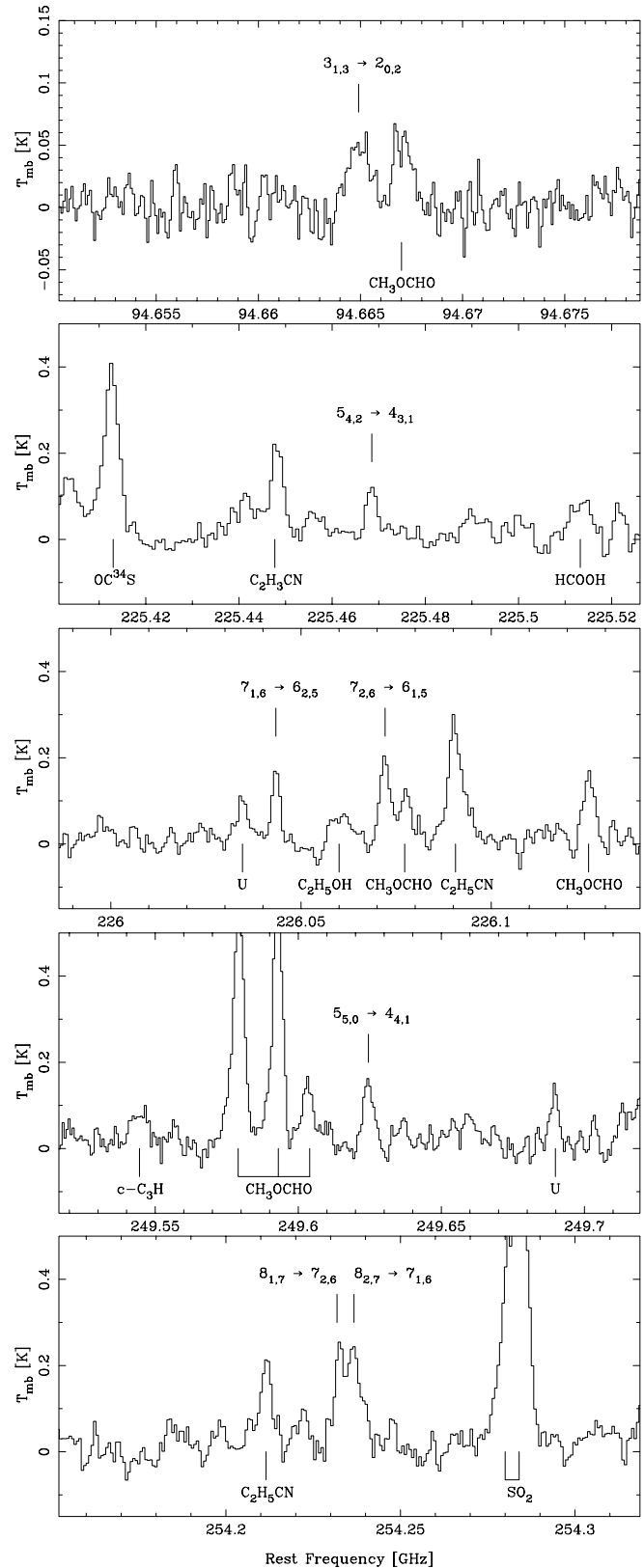


**Fig. 1.** Spectra towards NGC 6334F, with all seven detected  $c\text{-C}_2\text{H}_4\text{O}$  transitions indicated with their quantum numbers. Spectral lines of other molecules are labelled with the relevant species. The rest frequency scale is based on  $V_{\text{LSR}} = -7 \text{ km s}^{-1}$ .

**Table 1.** Source coordinates and radial velocities with respect to the local standard of rest,  $V_{\text{LSR}}$ .

Source	$\alpha(1950.0)$	$\delta(1950.0)$	$V_{\text{LSR}}$ [ $\text{km s}^{-1}$ ]
Orion 3'N	05 <sup>h</sup> 32 <sup>m</sup> 51.0 <sup>s</sup>	−05°20′50.0″	+9
G322.2+0.6	15 <sup>h</sup> 14 <sup>m</sup> 50.0 <sup>s</sup>	−56°28′00.0″	−56
G327.3−0.6	15 <sup>h</sup> 49 <sup>m</sup> 15.6 <sup>s</sup>	−54°28′07.0″	−45
G333.13−0.43	16 <sup>h</sup> 17 <sup>m</sup> 16.8 <sup>s</sup>	−50°28′17.0″	−52
G339.88−1.26	16 <sup>h</sup> 48 <sup>m</sup> 24.8 <sup>s</sup>	−46°03′33.9″	−39
NGC 6334F <sup>a</sup>	17 <sup>h</sup> 17 <sup>m</sup> 32.3 <sup>s</sup>	−35°44′02.5″	−7
G351.6−1.3	17 <sup>h</sup> 25 <sup>m</sup> 56.0 <sup>s</sup>	−36°37′54.0″	−12
M8 <sup>b</sup>	18 <sup>h</sup> 00 <sup>m</sup> 36.3 <sup>s</sup>	−24°22′53.0″	+10
G10.47+0.03 <sup>c</sup>	18 <sup>h</sup> 05 <sup>m</sup> 40.3 <sup>s</sup>	−19°52′21.0″	+68
G31.41+0.31	18 <sup>h</sup> 44 <sup>m</sup> 59.2 <sup>s</sup>	−01°16′07.0″	+97
G34.3+0.2	18 <sup>h</sup> 50 <sup>m</sup> 46.2 <sup>s</sup>	+01°11′13.0″	+58

<sup>a</sup> NGC 6334I, G351.41+0.64<sup>b</sup> NGC 6523<sup>c</sup> W31(1)

254 GHz). The corrected main-beam brightness temperature was subsequently calculated as  $T_{\text{mb}}/\eta_s$ , and if the spectral-line emission arises in a source having a Gaussian brightness distribution with a FWHM of 20″, this quantity will equal the peak brightness temperature of the source. If, on the other hand, the source size is larger than 20″ the true brightness temperature will be overestimated with this procedure. This discrepancy will be largest for the spectral lines with lowest frequencies, i.e. in the 3 mm band. Therefore, in case of extended emission, we will tend to underestimate the actual rotation temperatures of c-C<sub>2</sub>H<sub>4</sub>O and CH<sub>3</sub>CHO. However, we found that a single temperature fits the observed data significantly better with the described correction for beam-dilution. The adopted source size is in agreement with size estimates for G327 (Bergman 1992), G31 (Cesaroni et al. 1991), and G34 (Mehringer and Snyder 1996). No corrections for beam-filling were made to the C<sup>17</sup>O( $J=1\rightarrow 0$ ) line intensities.

We searched for seven transitions of c-C<sub>2</sub>H<sub>4</sub>O and three  $A/E$  pairs of transitions of CH<sub>3</sub>CHO in 11 sources (Table 1). Sample spectra can be found in Fig. 1. The lines were distributed over two frequency bands in the 3 mm band and four bands in the 1.3 mm band, and the transition data together with the SEST beam-width ( $\theta_{\text{mb}}$ ) at each frequency are listed in Table 2. The transitions were chosen to span a sufficient range of energies so that rotation temperatures and column densities could be reliably estimated (see Sect. 3). The rest frequencies,  $A$ -coefficients ( $A_{ul}$ ), and upper-state energies ( $E_u$ ) of c-C<sub>2</sub>H<sub>4</sub>O were calculated using the molecular constants reported by Hirose (1974), which were based on spectroscopic measurements between 10 and 124 GHz. The frequencies obtained in this way agree to within 0.5 MHz with recent laboratory measurements by Pan et al. (1998). For CH<sub>3</sub>CHO, we used the spectroscopic data of Kleiner, Lovas, & Godefroid (1996).

**Table 2.** Molecular transition data and beam sizes.

Rest freq. [MHz]	Transition [ $J_{K_a, K_c}$ ]	$E_u$ [K]	$A_{ul}$ [ $10^{-4} \text{ s}^{-1}$ ]	$\theta_{\text{mb}}$ [″]
c-C <sub>2</sub> H <sub>4</sub> O:				
94 664.6	3 <sub>1,3</sub> → 2 <sub>0,2</sub>	10	0.12	53
225 468.0	5 <sub>4,2</sub> → 4 <sub>3,1</sub>	33	1.06	22
226 043.1	7 <sub>1,6</sub> → 6 <sub>2,5</sub>	47	1.66	22
226 072.0	7 <sub>2,6</sub> → 6 <sub>1,5</sub>	47	1.66	22
249 623.6	5 <sub>5,0</sub> → 4 <sub>4,1</sub>	35	2.30	20
254 231.8	8 <sub>1,7</sub> → 7 <sub>2,6</sub>	59	2.48	20
254 235.7	8 <sub>2,7</sub> → 7 <sub>1,6</sub>	59	2.48	20
CH <sub>3</sub> CHO:				
112 248.7	6 <sub>1,6</sub> → 5 <sub>1,5</sub> $A++$	21	0.47	45
112 254.5	6 <sub>−1,6</sub> → 5 <sub>−1,5</sub> $E$	21	0.47	45
223 650.1	12 <sub>−1,12</sub> → 11 <sub>−1,11</sub> $E$	72	3.92	23
223 660.6	12 <sub>1,12</sub> → 11 <sub>1,11</sub> $A++$	72	3.92	23
249 323.9	13 <sub>2,12</sub> → 12 <sub>2,11</sub> $A--$	93	5.36	20
249 326.6	13 <sub>−2,12</sub> → 12 <sub>−2,11</sub> $E$	93	5.36	20

### 3. Analysis

The integrated intensity of a molecular transition  $u \rightarrow l$  can be calculated as

$$\int_{-\infty}^{\infty} T_{\text{b}} dv = \frac{hc^3}{8\pi k \nu_{ul}^2} A_{ul} g_u \frac{N}{Q(T_{\text{rot}})} e^{-E_u/kT_{\text{rot}}} \quad (1)$$

where  $T_{\text{b}}$  is the source brightness temperature,  $h$  is Planck's constant,  $c$  is the speed of light,  $k$  is Boltzmann's constant,  $\nu_{ul}$  is the transition frequency,  $A_{ul}$  is the Einstein  $A$ -coefficient,  $g_u$  is the statistical weight of the upper state of the transition,  $N$  is the column density of the species,  $T_{\text{rot}}$  is the rotation (Boltzmann) temperature,  $Q(T_{\text{rot}})$  is the partition function<sup>2</sup> evaluated at temperature  $T_{\text{rot}}$ , and  $E_u$  is the energy of the upper state. Three assumptions have been made to derive this equation: (i) the molecular energy levels are populated according to the Boltzmann distribution described by a temperature  $T_{\text{rot}}$ , (ii)  $1 - e^{-\tau_{ul}} \approx \tau_{ul}$ , where  $\tau_{ul}$  is the optical depth of a transition, and (iii) the brightness of the background radiation is negligible. Using the above relation to calculate the line intensities, we can infer a column density,  $N$ , and rotational excitation temperature,  $T_{\text{rot}}$ , and calculate the integrated intensity of each observed transition. To estimate how well the calculated line intensities fit the observed data we calculate the  $\chi^2$ -value for each set of parameters ( $T_{\text{rot}}$ ,  $N$ ) through

$$\chi^2 = \sum_{i=1}^n \left( \frac{I_i^{\text{obs}} - I_i^{\text{calc}}}{\sigma_i^{\text{obs}}} \right)^2 \quad (2)$$

where  $n$  is the number of data points,  $I_i^{\text{obs}}$  is the observed integrated line intensity,  $I_i^{\text{calc}}$  is the integrated line intensity predicted by the model, and  $\sigma_i^{\text{obs}}$  is the total uncertainty (spectral

<sup>2</sup> To calculate correctly the line intensity it is important that the statistical weights,  $g_u$ , are the same as those used when evaluating the partition function,  $Q(T)$ . In Appendix A we summarise the weights and partition functions used.

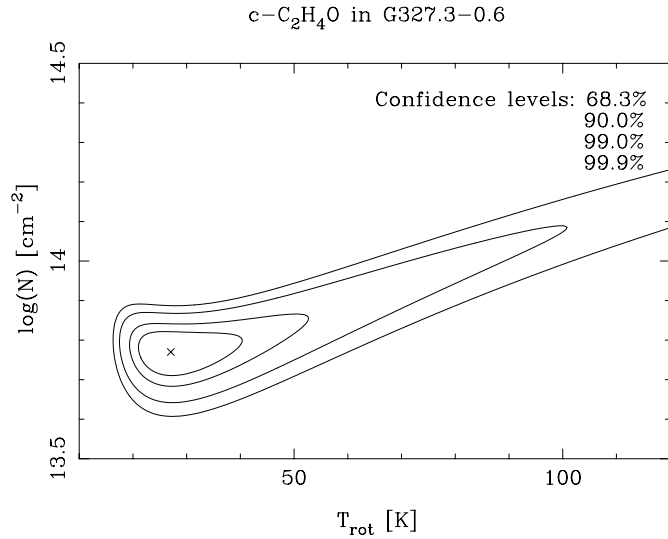


**Fig. 2.** The  $\chi^2$ -value as a function of the c-C<sub>2</sub>H<sub>4</sub>O column density  $N$  and rotation temperature  $T_{\text{rot}}$ . The set of parameters ( $T_{\text{rot}}$ ,  $N$ ) which gives minimum  $\chi^2$  is indicated with an x. The 68.3% contour level corresponds to  $1\sigma$ .

noise + pointing/calibration errors) of the observed line intensity. In the parameter plot in Fig. 2 the best fit, i.e. the set of parameters ( $T_{\text{rot}}$ ,  $N$ ) giving minimum  $\chi^2$ , has been indicated. Also drawn in the plot are the regions

$$\chi^2 \leq \chi_{\text{min}}^2 + \Delta\chi^2$$

for  $\Delta\chi^2$  values equal to 2.3, 4.6, 9.2, and 13.8. Assuming that all measurements are distributed according to the normal distribution, the probability of enclosing the correct parameters  $T_{\text{rot}}$  and  $N$  is 68.3%, 90%, 99%, and 99.9%, for each of the  $\Delta\chi^2$  values, respectively (Lampton, Margon, & Bowyer 1976). The 68.3% contour corresponds to  $1\sigma$  uncertainty.

Compared to a regular least-squares fitting procedure, this method gives more appropriate constraints on the estimated column density and excitation temperature. A consequence of this fitting procedure is that solutions ( $T_{\text{rot}}$ ,  $N$ ) producing line intensities that are less than the observed intensities are favoured, since the contribution to the  $\chi^2$ -value of each data point,  $\chi_i^2$ , is

$$\chi_i^2 = \left( \frac{I_i^{\text{obs}} - I_i^{\text{calc}}}{\sigma_i^{\text{obs}}} \right)^2 \rightarrow \left( \frac{I_i^{\text{obs}}}{\sigma_i^{\text{obs}}} \right)^2 \quad \text{when } I_i^{\text{calc}} \rightarrow 0.$$

However, for  $I_i^{\text{calc}} > I_i^{\text{obs}}$ ,  $\chi_i^2$  is unlimited. Hence, large model intensities are in general given more penalty relative to small model intensities. What limits the accuracy of the applied model is, in most cases, that the excitation cannot be described by a single Boltzmann temperature rather than the uncertainty in the line intensities. Deviations from a single temperature can have several causes: variations in the beam-filling between the transitions; excitation gradients along the line-of-sight; radiative pumping; or subthermal excitation. For most analysed molecules, the estimated column density is rather insensitive to the rotation temperature, as can be seen in the plot of the  $\chi^2$  distribution diagram in Fig. 2.

Taking the natural logarithm of each side of Eq. 1, we arrive at

$$\ln \left( \frac{8\pi k\nu_{ul}^2}{hc^3 A_{ul} g_u} \int_{-\infty}^{+\infty} T_b dv \right) = \ln \left( \frac{N}{Q(T_{\text{rot}})} \right) - \frac{E_u}{kT_{\text{rot}}} \quad (3)$$

A rotation diagram can be constructed by plotting the left-hand quantity against  $E_u$  for each observed transition, and under ideal conditions the data points will form a straight line. The inverse of the negative slope of the line is equal to the rotation temperature, and the line intercept with the  $y$ -axis equals  $\ln(N/Q(T_{\text{rot}}))$ . However, in this paper we only use the rotation diagrams to present the data, not for the analysis itself.

## 4. Results

### 4.1. General

Ethylene oxide was securely detected, through three or more transitions, towards four sources (NGC 6334F, G327, G31, and G34), and tentatively detected in one transition towards G10 (Table 3). Acetaldehyde was found in NGC 6334F, G327, G31, G34, G322, and Orion 3'N (Table 4), and was always found to be more abundant than ethylene oxide.

In Fig. 1 all c-C<sub>2</sub>H<sub>4</sub>O spectra taken towards NGC 6334F are shown. The rms noise in the spectra is 15 – 25 mK per channel ( $T_{\text{mb}}$ ), and the number of detected spectral lines is more than 200 for some of the sources. A large fraction of these lines are unidentified. The probability for line overlapping, and hence confusion, is much less in these sources than in, for example, Sgr B2(N) (Nummelin et al. 1998a) because of the significantly smaller line widths ( $\sim 5 \text{ km s}^{-1}$ ). This enables more reliable line identifications and makes these sources excellent for multilevel analyses.

The radial velocities of the c-C<sub>2</sub>H<sub>4</sub>O and CH<sub>3</sub>CHO spectral lines are consistent to within 2 km s<sup>-1</sup> and agree well with velocities measured for lines from other molecules towards all of the sources. In case we failed to detect an observed line, a  $3\sigma$  upper limit to the integrated intensity was calculated using 7 km s<sup>-1</sup> (the full linewidth at 25% of maximum intensity) as the assumed line width for all sources except Orion 3'N, where 3 km s<sup>-1</sup> was used. No upper limits were included in the  $\chi^2$ -fitting procedure.

In order to estimate the fractional molecular abundances relative to H<sub>2</sub> we have calculated the beam-averaged H<sub>2</sub> column density from the integrated intensity of the C<sup>17</sup>O( $J=1 \rightarrow 0$ ) line at 112 359 MHz, which was located within the wide-band AOS spectrum centred on the CH<sub>3</sub>CHO( $6_{1,6} \rightarrow 5_{1,5}$ ) line towards 5 of the sources (NGC 6334F, G327, G31, G10, and G322). The H<sub>2</sub> column density was calculated as

$$N(\text{H}_2) = \frac{X[^{18}\text{O}]}{X[^{17}\text{O}]X[^{18}\text{O}]} \times N(\text{C}^{17}\text{O})$$

where we have assumed that  $X[^{18}\text{O}]/X[^{17}\text{O}]=3.65$  (Penzias 1981),  $X[^{18}\text{O}] \equiv N(\text{C}^{18}\text{O})/N(\text{H}_2)=2 \times 10^{-7}$  (Frerking, Langer, & Wilson 1982), and that C<sup>17</sup>O is optically thin. The resulting H<sub>2</sub> column densities (Table 5)

**Table 3.** c-C<sub>2</sub>H<sub>4</sub>O line intensities and upper limits

Source	$\int T_{\text{mb}} dv$ [K km s <sup>-1</sup> ]						
	3 <sub>1,3</sub> → 2 <sub>0,2</sub>	5 <sub>4,2</sub> → 4 <sub>3,1</sub>	7 <sub>1,6</sub> → 6 <sub>2,5</sub>	7 <sub>2,6</sub> → 6 <sub>1,5</sub>	5 <sub>5,0</sub> → 4 <sub>4,1</sub>	8 <sub>1,7</sub> → 7 <sub>2,6</sub>	8 <sub>2,7</sub> → 7 <sub>1,6</sub>
Orion 3'N	< 0.04	< 0.07	< 0.07	< 0.07	< 0.14	...	...
G322.2+0.6	...	...	...	...	< 0.25	...	...
G327.3-0.6	0.15±0.01	0.35±0.04	0.31±0.04	0.43±0.04	0.52±0.05	0.61±0.05	0.59±0.05
G333.13-0.43	< 0.08	...	...	...	< 0.16	...	...
G339.88-1.26	< 0.07	...	...	...	< 0.17	...	...
NGC 6334F	0.20±0.02	0.49±0.04	0.62±0.05	0.90±0.05	0.87±0.07	1.05±0.05	1.06±0.05
G351.6-1.3	< 0.10	...	...	...	< 0.21	...	...
M8	< 0.11	...	...	...	< 0.28	...	...
G10.47+0.03	< 0.10	< 0.18	< 0.18	< 0.18	0.31±0.04 <sup>a</sup>	< 0.24	< 0.24
G31.41+0.31	0.10±0.02	0.34±0.06	0.45±0.07	0.74±0.07	0.54±0.06	0.51±0.04	0.44±0.04
G34.3+0.2	< 0.09	< 0.13	0.47±0.06	...	0.39±0.05	0.48±0.06 <sup>b</sup>	

<sup>a</sup> Tentative detection.<sup>b</sup> Blend.**Table 4.** CH<sub>3</sub>CHO line intensities and upper limits

Source	$\int T_{\text{mb}} dv$ [K km s <sup>-1</sup> ]					
	6 <sub>1,6</sub> → 5 <sub>1,5</sub>		12 <sub>1,12</sub> → 11 <sub>1,11</sub>		13 <sub>2,12</sub> → 12 <sub>2,11</sub>	
	<i>A</i>	<i>E</i>	<i>A</i>	<i>E</i>	<i>A</i>	<i>E</i>
Orion 3'N	0.23±0.01	0.16±0.01	< 0.07	< 0.07	< 0.14	
G322.2+0.6	0.42±0.01	0.34±0.01	...	...	< 0.16	
G327.3-0.6	1.51±0.03	1.82±0.03	1.55±0.05	2.09±0.05	0.91±0.05	0.74±0.05
G333.13-0.43	...	...	...	...	< 0.16	
G339.88-1.26	...	...	...	...	< 0.17	
NGC 6334F	0.82±0.03	0.90±0.03	1.11±0.03	1.28±0.03	0.89±0.07 <sup>a</sup>	
G351.6-1.3	...	...	...	...	< 0.21	
M8	...	...	...	...	< 0.28	
G10.47+0.03	0.46±0.03	0.70±0.04	0.81±0.08	1.18±0.10	2.03±0.09 <sup>a</sup>	
G31.41+0.31	0.41±0.03	0.58±0.04	0.79±0.06	0.99±0.06	1.49±0.07 <sup>a</sup>	
G34.3+0.2	0.79±0.02	0.85±0.02	0.73±0.06	0.79±0.06	0.95±0.08 <sup>a</sup>	

<sup>a</sup> *A* and *E* components blended.

agree well with published results for NGC 6334F (based on 400 μm dust continuum; Gezari 1982) and G327 (based on C<sup>18</sup>O(*J*=2→1); Bergman 1992).

Four of the targeted lines appear in blended doublets: the 8<sub>1,7</sub>→7<sub>2,6</sub> and 8<sub>2,7</sub>→7<sub>1,6</sub> lines of c-C<sub>2</sub>H<sub>4</sub>O, and the 13<sub>2,12</sub>→12<sub>2,11</sub> *A* and *E* components of CH<sub>3</sub>CHO. The lines in the c-C<sub>2</sub>H<sub>4</sub>O pair are resolved or marginally resolved in NGC 6334F and G327, while the CH<sub>3</sub>CHO doublet is unresolved in all sources (see discussion of each source).

We derived rotation temperatures and column densities for c-C<sub>2</sub>H<sub>4</sub>O and CH<sub>3</sub>CHO using the χ<sup>2</sup>-fitting procedure described in the previous section, and the data are presented in rotation diagram format in Fig. 3. In each diagram we have also indicated the rotation temperature and column density giving the minimum χ<sup>2</sup>-value (dotted/solid lines). For CH<sub>3</sub>CHO, the column densities include both the *A* and *E* species. The resulting excitation temperatures, molecular column densities

averaged over a 20'' source, and fractional abundances relative to H<sub>2</sub> for each source can be found in Table 6. In the following subsections we summarise the results for each source.

#### 4.2. NGC 6334F

The NGC 6334 giant molecular cloud complex is located at a distance of 1.7 kpc from the sun (Neckel 1978). It contains multiple centres of high-mass star formation, traced at various wavelengths by H II regions, OB-stars, OH and H<sub>2</sub>O masers, and molecular outflows. Roman numerals as well as alphabetical systems are used to designate the different continuum sources. The position we chose to observe was NGC 6334F, an optically obscured compact (0.02 pc) H II region with cometary morphology (Gaume & Mutel 1987).

In NGC 6334F, all seven observed transitions of c-C<sub>2</sub>H<sub>4</sub>O were detected (Fig. 1). The intensity ratio of the 7→6 para/ortho

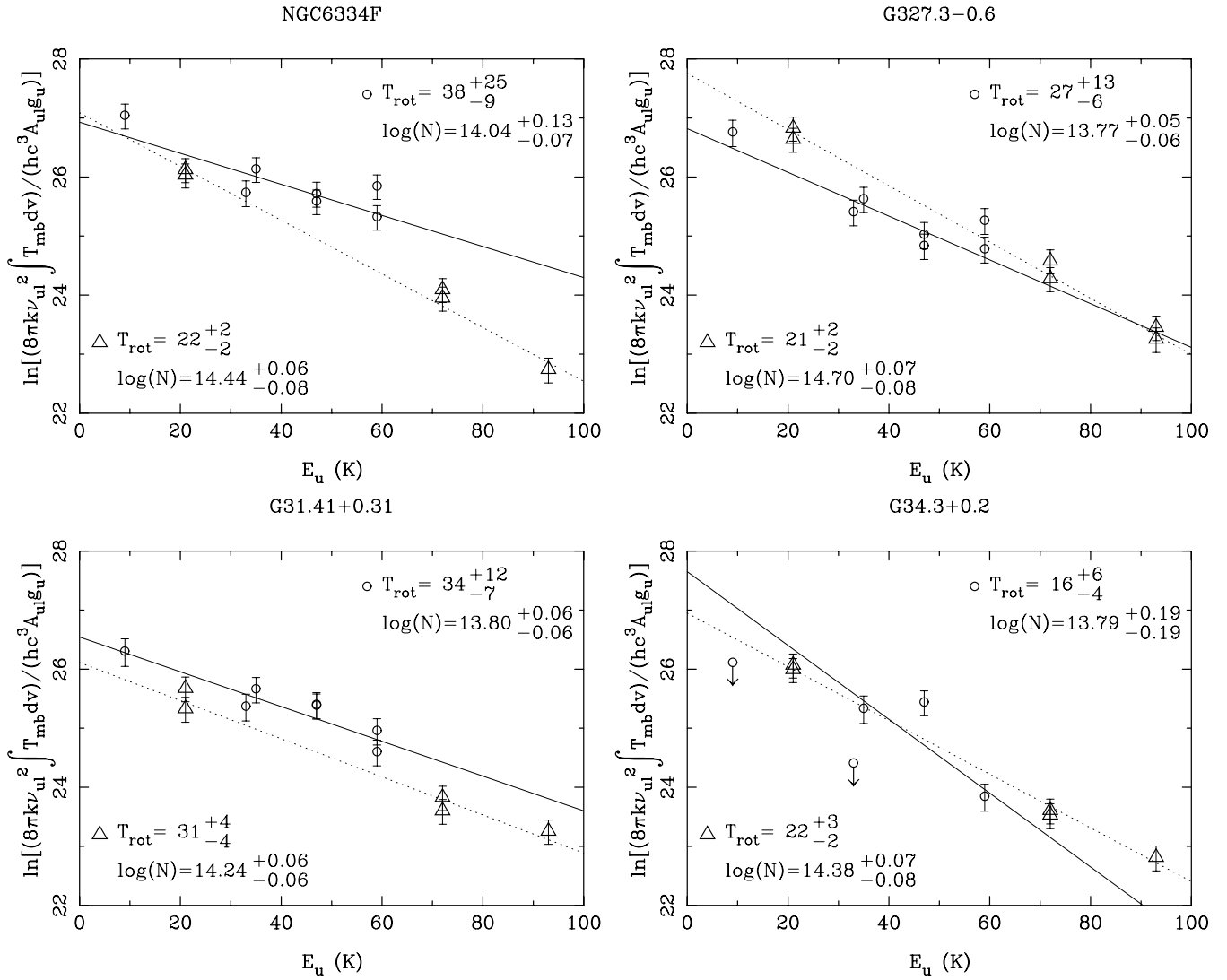


**Fig. 3.** Rotation diagrams for ethylene oxide (circles) and acetaldehyde (triangles), where the best-fitting parameters  $T_{rot}$  and  $N$ , obtained from the  $\chi^2$ -minimisation procedure, have been indicated for each molecule in each source with solid lines ( $C_2H_4O$ ) and dotted lines ( $CH_3CHO$ ). The best-fit values for  $C_2H_4O$  are given in the upper right corner and those for  $CH_3CHO$  in the lower left corner of each diagram. The errors given on  $T_{rot}$  and  $N$  are  $1\sigma$ .

**Table 5.**  $C^{17}O(J=1\rightarrow 0)$  results

Source	$\int T_{mb} dv$ [K km s $^{-1}$ ]	$N(C^{17}O)^a$ [cm $^{-2}$ ]	$N(H_2)^b$ [cm $^{-2}$ ]
G322.2+0.6	5.0	$8.2 \times 10^{15}$	$1.5 \times 10^{23}$
G327.3-0.6	6.6	$1.1 \times 10^{16}$	$2.0 \times 10^{23}$
G31.41+0.31	5.4	$8.8 \times 10^{15}$	$1.6 \times 10^{23}$
NGC 6334F	6.8	$1.1 \times 10^{16}$	$2.0 \times 10^{23}$
G10.47+0.03	4.5	$7.3 \times 10^{15}$	$1.3 \times 10^{23}$

<sup>a</sup> Assuming  $T_{ex}(C^{17}O)=30$  K for all sources.

<sup>b</sup> Using  $X[C^{17}O]=5.5 \times 10^{-8}$  (see text).

doublet approximately equals its (optically thin) equilibrium value, i.e. the statistical weight ratio of 6:10, but the ratio of the 8 $\rightarrow$ 7 doublet is approximately 1:1. We believe there can be two reasons for this. First, transitions from the ortho and para species frequently occur in pairs, with the lines mutually blended, which allows line radiation to be “accidentally” exchanged between the two species. In the  $\lambda 15$  cm –  $\lambda 0.1$  mm wavelength range there is about one such pair (with  $\Delta\nu < 4$  MHz) per 10 transitions. This could change the intensity ratio between the ortho and para lines from the theoretically expected value of 10:6. Second, the  $8_{2,7} \rightarrow 7_{1,6}$  transition (at 254 235 MHz) coincides in frequency with the  $44_{5,39} \rightarrow 44_{4,40}$  transition ( $E_u=950$  K) of dimethyl ether ( $CH_3OCH_3$ ; Groner et al. 1998). Although the rotation temperature of the high-temperature component of  $CH_3OCH_3$  is rather poorly constrained (see discussion of  $CH_3OCH_3$  below), and the intensity of this transition is correspondingly diffi-

cult to determine accurately, we believe that the  $44_{5,39} \rightarrow 44_{4,40}$  line could contribute significantly to the measured intensity of the line feature at 254 235 MHz. Since NGC 6334F has the highest observed column density of  $\text{CH}_3\text{OCH}_3$  in the high-temperature component, we estimate that the contribution from the  $44_{5,39} \rightarrow 44_{4,40}$  line to the emission at 254 235 MHz is less significant towards the other sources.

In  $\text{CH}_3\text{CHO}$  all six targeted transitions were detected, together with the  $13_{2,12} \rightarrow 12_{2,11}$  transition in the first torsionally excited state ( $E_u=298$  K). This line was, however, excluded from the analysis and the rotation diagram since the excitation of the torsionally excited states is believed to differ from that of the ground state transitions (e.g. Lovas et al. 1982).

#### 4.3. G327.3–0.6

The G327.3–0.6 region was first observed as a peak in the radio continuum at 408 MHz and 5 GHz (Shaver & Goss 1970) and is also a source of strong infrared emission (Kuiper et al. 1987). There are prominent  $\text{H}_2\text{O}$ - and  $\text{OH}$ -masers (Batchelor et al. 1980; Caswell, Haynes, & Goss 1980) associated with this cloud. The kinematical distance to G327 is 2.9 kpc (Simpson & Rubin 1990). In a detailed study of  $\text{CH}_3\text{CN}$  and  $\text{CH}_3\text{C}_2\text{H}$  with SEST Bergman (1992) found two adjacent dense cores in this molecular cloud: one cold (kinetic temperature  $T_k=30$  K) cloud core, and one hot ( $T_k=100\text{--}200$  K) core. The latter position was observed in the present survey.

As was the case for NGC 6334F, ethylene oxide as well as acetaldehyde were detected in all transitions. The  $c\text{-C}_2\text{H}_4\text{O}$   $8 \rightarrow 7$  doublet feature is slightly double-peaked but the two components are poorly resolved and hence the line ratio cannot be determined with any accuracy. The  $\text{CH}_3\text{CHO}$   $13_{2,12} \rightarrow 12_{2,11}$  *A* and *E* components are unresolved although two Gaussian components could be fitted to the line feature.

#### 4.4. G31.41+0.31

G31.41+0.31 is an H II region with cometary morphology at a kinematical distance of 7.9 kpc from the sun (Churchwell, Walmsley, & Cesaroni 1990), and has been found to contain hot and dense gas (Olm, Cesaroni, & Walmsley 1996). Ethylene oxide and acetaldehyde were detected in all targeted transitions. Similar to G327, the  $c\text{-C}_2\text{H}_4\text{O}$   $8 \rightarrow 7$  line doublet is unresolved but a fit using two Gaussian components was forced to the line feature.

#### 4.5. G34.3+0.2

G34.3+0.2 is, similar to NGC 6334F and G31, a cometary H II region (Gaume, Fey, & Clausen 1994) at a kinematical distance of 3.1 kpc. The physics and chemistry of the hot molecular core in G34 has been investigated in detail by Millar, Macdonald, & Gibb (1997). Based on their three-component model of this source we estimate the  $\text{H}_2$  column density to be  $3 \times 10^{23} \text{ cm}^{-2}$ . No  $\text{C}^{17}\text{O}(J=1 \rightarrow 0)$  spectrum was observed towards G34.

The  $c\text{-C}_2\text{H}_4\text{O}$   $8 \rightarrow 7$  doublet was not resolved in this source, and only one Gaussian component was fitted to the line feature. The  $7_{2,6} \rightarrow 6_{1,5}$  line is severely blended with the  $10_{3,7} \rightarrow 9_{1,8}$  transition of  $\text{CH}_3\text{OCHO}$ ; therefore, no line intensity could be estimated. The  $5_{4,2} \rightarrow 4_{3,1}$  line was not detected at a noise level of 15 mK. However, due to a forest of weak ( $< 50$  mK) lines or a small baseline variation, the true noise level is difficult to estimate in this spectral region.

#### 4.6. Other sources

In G10.47+0.03 we have tentatively assigned a line feature at 249 325.2 MHz to the  $5_{5,0} \rightarrow 4_{4,1}$  transition of ethylene oxide. No other  $c\text{-C}_2\text{H}_4\text{O}$  transitions, but all targeted lines of acetaldehyde, were detected in this source. Towards Orion 3'N and G322.2+0.6 the  $6_{1,6} \rightarrow 5_{1,5}$  *A/E* pair of transitions of  $\text{CH}_3\text{CHO}$  were detected.

#### 4.7. Other molecular species detected

In the high signal-to-noise  $c\text{-C}_2\text{H}_4\text{O}$  and  $\text{CH}_3\text{CHO}$  spectra we coincidentally detected several other large asymmetric molecules, e.g.  $\text{CH}_3\text{OCH}_3$ ,  $\text{C}_2\text{H}_5\text{OH}$ ,  $\text{HCOOH}$  and  $\text{CH}_3\text{OH}$ . Molecules with sufficient numbers of lines detected were analysed with the  $\chi^2$ -minimisation method described in Sect. 3 and the resulting rotation temperature, column density, and fractional abundance of each of these species are tabulated in Table 6. The rotation diagrams for each species can be found in Fig. 4 and a brief discussion is given below. Although we detected quite a large number of lines from methyl formate ( $\text{CH}_3\text{OCHO}$ ) and ethyl cyanide ( $\text{C}_2\text{H}_5\text{CN}$ ), these species were not analysed in this paper since their excitations could not be characterised well even with two-temperature models and, hence, no reliable column densities could be determined (cf. Turner 1991).

##### 4.7.1. $\text{CH}_3\text{OH}$

Methanol ( $\text{CH}_3\text{OH}$ ) was detected in 7 sources: G333, G339, NGC 6334F, G327, G31, G34, and G10. In G333 and G339 4 lines were detected, with upper state energies between 145 and 328 K, and in the rest of the sources 8 or 9 transitions, covering energies 19 – 377 K, were detected. All  $\text{CH}_3\text{OH}$  transitions are in the 1.3 mm band. In NGC 6334F the  $10_7 \rightarrow 9_6$  line in the first torsionally excited state ( $E_u=707$  K) was also detected, but this line was excluded from the analysis since the excitation mechanism for this line probably differs from that of the ground state lines (e.g. Lovas et al. 1982). At the excitation temperatures deduced, about 80 K for all of the sources, the contribution from the torsional part to the total partition function is only a few percent and has therefore been neglected in the calculation of the column densities.

4.7.2. CH<sub>3</sub>OCH<sub>3</sub>

Dimethyl ether (CH<sub>3</sub>OCH<sub>3</sub>) was detected in NGC 6334F, G327, G31, G34, and G10 through 5 transitions with energies in the range 38 – 330 K. The splitting of CH<sub>3</sub>OCH<sub>3</sub> into its four torsional substates *AA*, *AE*, *EA*, and *EE* was not resolved in any of the sources. In NGC 6334F and G327 two physical components, each characterised by a rotation temperature and CH<sub>3</sub>OCH<sub>3</sub> column density, seem to be required to fit the observational data. The low-temperature components were in both cases set to 20 K, but the values of both rotation temperatures are rather uncertain. In Table 6 the 20 K component was used to calculate the fractional abundance, since its rotation temperature is similar to that of ethylene oxide and acetaldehyde. The difference in column densities between the two components is small in both sources.

The rotation diagrams for G31, G34 and G10 also show some dichotomy similar to that seen in NGC 6334F and G327, but, since it is less pronounced, these data were reasonably fitted using a single temperature. All of the CH<sub>3</sub>OCH<sub>3</sub> transitions are in the 1.3 mm wavelength band and the low-temperature component can therefore not be attributed to an over-corrected beam-filling.

4.7.3. C<sub>2</sub>H<sub>5</sub>OH

Most of the detected transitions of ethanol (C<sub>2</sub>H<sub>5</sub>OH) are relatively weak and the number of lines above the noise level therefore varies between three (G10) and seven (G31). In G10 the excitation temperature was forced to be 100 K to allow a crude estimate of the column density. The 7<sub>3,5</sub>→7<sub>2,5</sub> transition ( $E_u=96$  K) appears too strong relative to the other lines in most of the sources, and, since the line is unusually broad, it may be blended with some unidentified line. One of the transitions detected ( $E_u=35$  K) belongs to ethanol in the *trans* torsional substate, whereas the other lines belong to the *gauche+* and *gauche-* substates (offset 57 K and 62 K from the *trans* state, respectively). We used the three-substate partition function given by Pearson et al. (1997). The fractional abundance derived for G34 agrees well with the results of Millar, Macdonald, & Habing (1995), although our rotation temperature and column density are somewhat lower.

## 4.7.4. HCOOH

Three transitions of formic acid (HCOOH), one of which is in the 3 mm band ( $E_u=29$  K), were detected in NGC 6334F, G327, G31, and G10. The rotation temperatures and column densities are rather poorly constrained because of the few lines detected.

## 5. Discussion

## 5.1. Molecular excitation and abundances

The sources where we detected ethylene oxide are similar in the sense that they are all compact (<0.5 pc) and dense hot cores within massive star-forming regions, and have high abundances

**Table 6.** Rotation temperatures, column densities, and fractional abundances relative to H<sub>2</sub>

	$T_{\text{rot}}$ [K]	$\log(N)^a$ [cm <sup>-2</sup> ]	$X$
NGC 6334F			
c-C <sub>2</sub> H <sub>4</sub> O	38 <sup>+25</sup> <sub>-9</sub>	14.04 <sup>+0.13</sup> <sub>-0.07</sub>	6 × 10 <sup>-10</sup>
CH <sub>3</sub> CHO	22 <sup>+2</sup> <sub>-2</sub>	14.44 <sup>+0.06</sup> <sub>-0.08</sub>	1 × 10 <sup>-9</sup>
CH <sub>3</sub> OCH <sub>3</sub>	20/440	15.5/16.1	2 × 10 <sup>-8b</sup>
C <sub>2</sub> H <sub>5</sub> OH	94 <sup>+44</sup> <sub>-20</sub>	15.15 <sup>+0.13</sup> <sub>-0.11</sub>	7 × 10 <sup>-9</sup>
CH <sub>3</sub> OH	79 <sup>+21</sup> <sub>-8</sub>	16.49 <sup>+0.10</sup> <sub>-0.17</sub>	2 × 10 <sup>-7</sup>
HCOOH	34 <sup>+24</sup> <sub>-8</sub>	14.25 <sup>+0.09</sup> <sub>-0.10</sub>	9 × 10 <sup>-10</sup>
G327.3–0.6			
c-C <sub>2</sub> H <sub>4</sub> O	27 <sup>+13</sup> <sub>-6</sub>	13.77 <sup>+0.05</sup> <sub>-0.06</sub>	3 × 10 <sup>-10</sup>
CH <sub>3</sub> CHO	21 <sup>+2</sup> <sub>-2</sub>	14.70 <sup>+0.07</sup> <sub>-0.08</sub>	3 × 10 <sup>-9</sup>
CH <sub>3</sub> OCH <sub>3</sub>	20/500	15.4/16.0	1 × 10 <sup>-8b</sup>
C <sub>2</sub> H <sub>5</sub> OH	95 <sup>+41</sup> <sub>-20</sub>	15.17 <sup>+0.10</sup> <sub>-0.08</sub>	8 × 10 <sup>-9</sup>
CH <sub>3</sub> OH	70 <sup>+12</sup> <sub>-8</sub>	16.27 <sup>+0.11</sup> <sub>-0.15</sub>	1 × 10 <sup>-7</sup>
HCOOH	20 <sup>+7</sup> <sub>-4</sub>	14.23 <sup>+0.15</sup> <sub>-0.21</sub>	9 × 10 <sup>-10</sup>
G31.41+0.31			
c-C <sub>2</sub> H <sub>4</sub> O	34 <sup>+12</sup> <sub>-4</sub>	13.80 <sup>+0.06</sup> <sub>-0.06</sub>	4 × 10 <sup>-10</sup>
CH <sub>3</sub> CHO	31 <sup>+4</sup> <sub>-4</sub>	14.24 <sup>+0.06</sup> <sub>-0.06</sub>	1 × 10 <sup>-9</sup>
CH <sub>3</sub> OCH <sub>3</sub>	166 <sup>+58</sup> <sub>-37</sub>	15.55 <sup>+0.09</sup> <sub>-0.09</sub>	2 × 10 <sup>-8</sup>
C <sub>2</sub> H <sub>5</sub> OH	103 <sup>+41</sup> <sub>-20</sub>	15.41 <sup>+0.11</sup> <sub>-0.07</sub>	2 × 10 <sup>-8</sup>
CH <sub>3</sub> OH	82 <sup>+12</sup> <sub>-8</sub>	16.13 <sup>+0.08</sup> <sub>-0.11</sub>	9 × 10 <sup>-8</sup>
HCOOH	39 <sup>+57</sup> <sub>-11</sub>	14.16 <sup>+0.12</sup> <sub>-0.10</sub>	1 × 10 <sup>-9</sup>
G34.3+0.2			
c-C <sub>2</sub> H <sub>4</sub> O	16 <sup>+4</sup> <sub>-4</sub>	13.78 <sup>+0.19</sup> <sub>-0.19</sub>	2 × 10 <sup>-10</sup>
CH <sub>3</sub> CHO	22 <sup>+3</sup> <sub>-2</sub>	14.38 <sup>+0.07</sup> <sub>-0.08</sub>	8 × 10 <sup>-10</sup>
CH <sub>3</sub> OCH <sub>3</sub>	152 <sup>+48</sup> <sub>-32</sub>	15.54 <sup>+0.08</sup> <sub>-0.08</sub>	1 × 10 <sup>-8</sup>
C <sub>2</sub> H <sub>5</sub> OH	70 <sup>+22</sup> <sub>-12</sub>	15.08 <sup>+0.06</sup> <sub>-0.08</sub>	4 × 10 <sup>-9</sup>
CH <sub>3</sub> OH	79 <sup>+13</sup> <sub>-8</sub>	16.39 <sup>+0.09</sup> <sub>-0.11</sub>	8 × 10 <sup>-8</sup>
HCOOH	...	...	...
G10.47+0.03			
c-C <sub>2</sub> H <sub>4</sub> O	...	<13.6 <sup>c</sup>	< 3 × 10 <sup>-10</sup>
CH <sub>3</sub> CHO	31 <sup>+7</sup> <sub>-4</sub>	14.29 <sup>+0.06</sup> <sub>-0.07</sub>	1 × 10 <sup>-9</sup>
CH <sub>3</sub> OCH <sub>3</sub>	147 <sup>+39</sup> <sub>-29</sub>	15.63 <sup>+0.07</sup> <sub>-0.08</sub>	3 × 10 <sup>-8</sup>
C <sub>2</sub> H <sub>5</sub> OH	100 <sup>d</sup>	15.22 <sup>+0.09</sup> <sub>-0.11</sub>	1 × 10 <sup>-8</sup>
CH <sub>3</sub> OH	81 <sup>+11</sup> <sub>-8</sub>	16.42 <sup>+0.08</sup> <sub>-0.11</sub>	2 × 10 <sup>-7</sup>
HCOOH	27 <sup>+24</sup> <sub>-6</sub>	14.17 <sup>+0.13</sup> <sub>-0.16</sub>	1 × 10 <sup>-9</sup>

<sup>a</sup> The column densities and abundances listed assume a 20'' source size

<sup>b</sup> Abundance calculated for the 20 K component

<sup>c</sup> Assuming  $T_{\text{rot}}=30$  K

<sup>d</sup>  $T_{\text{rot}}$  forced to 100 K (see text)

of large saturated molecules. In the sources where neither c-C<sub>2</sub>H<sub>4</sub>O nor CH<sub>3</sub>CHO was detected, no other molecules were detected in the observed bands with the exception of CH<sub>3</sub>OH, which was weakly detected in G333 and G339.

Both the rotation temperature and column density of each species are very similar in the different sources. The deduced rotation temperatures can be divided into three temperature ranges: 15 – 40 K (c-C<sub>2</sub>H<sub>4</sub>O, CH<sub>3</sub>CHO, HCOOH, and

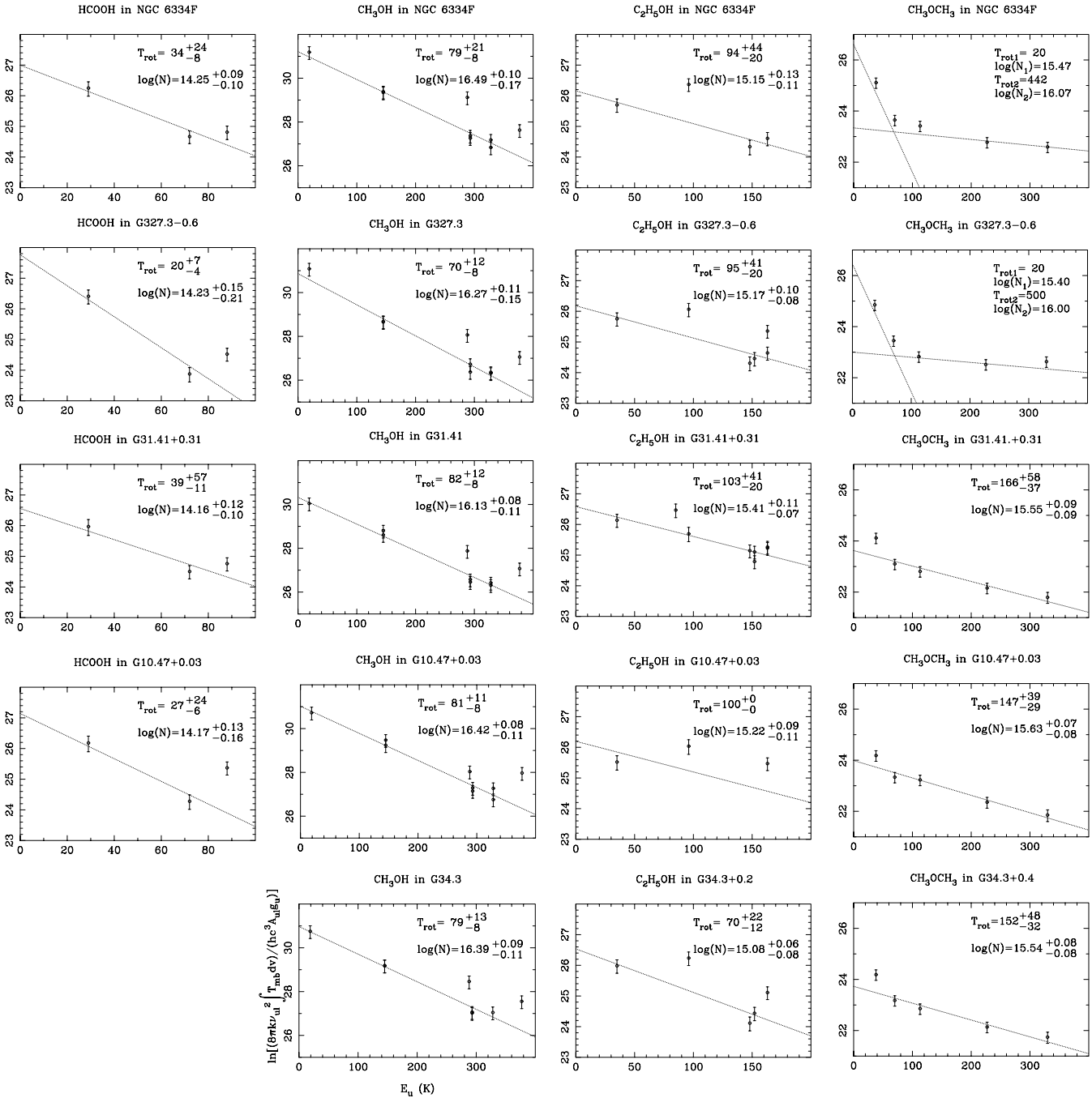


**Fig. 4.** Rotation diagrams for HCOOH, CH<sub>3</sub>OH, C<sub>2</sub>H<sub>5</sub>OH, and CH<sub>3</sub>OCH<sub>3</sub>, each in a separate column. The dotted lines indicate the column densities and rotational excitation temperatures obtained through the  $\chi^2$ -minimisation method described in Sect. 3, and are not fits in the logarithmic rotation diagrams directly.

CH<sub>3</sub>OCH<sub>3</sub>), 70 – 100 K (CH<sub>3</sub>OH and C<sub>2</sub>H<sub>5</sub>OH), and 400 – 500 K (CH<sub>3</sub>OCH<sub>3</sub>). These effects seem to indicate that the molecular line emission arises in regions with different physical conditions. However, some caution is necessary since the higher rotation temperatures (CH<sub>3</sub>OH, C<sub>2</sub>H<sub>5</sub>OH) are mostly based on lines with excitation energies above 100 K, whereas the low rotation temperatures (c-C<sub>2</sub>H<sub>4</sub>O, CH<sub>3</sub>CHO, HCOOH) were deduced entirely from low-energy (<100 K) lines.

In his analysis of the emission from CH<sub>3</sub>CN and CH<sub>3</sub>C<sub>2</sub>H in the hot core in G327, Bergman (1992) identifies a compact core, 0.06 pc in diameter, with inwardly increasing kinetic temperature (100 – 200 K) and H<sub>2</sub> density ( $10^6$  –  $10^8$  cm<sup>-3</sup>). This core is surrounded by a cooler (40 – 60 K), less dense ( $10^5$  –  $10^6$  cm<sup>-3</sup>) envelope, ~0.3 pc in diameter. Qualitatively, this physical structure is probably valid for the other hot-core sources as well. The rotation temperatures deduced for c-C<sub>2</sub>H<sub>4</sub>O and CH<sub>3</sub>CHO, 20

– 40 K, suggest emission mainly originating in the cooler envelope. However, the rotation temperatures are not necessarily equal to the kinetic temperatures. Although an accurate determination of the critical density ( $n_{\text{crit}}$ ) requires knowledge of the collision rate coefficients and solution of the statistical equilibrium equations, we estimate that  $n_{\text{crit}}$  may be as high as  $10^6$  –  $10^7$   $\text{cm}^{-3}$  for the  $c\text{-C}_2\text{H}_4\text{O}$  and  $\text{CH}_3\text{CHO}$  transitions with the higher  $A$ -coefficients. It is thus plausible that the excitation of these species can be significantly subthermal. Furthermore, in our line survey of the hot cores in Sgr B2 two temperature components are clearly visible in  $\text{CH}_3\text{CHO}$ , thus indicating its presence in both the hot and cold gas (Nummelin et al. 1998a, 1998b). Since at least one torsionally excited line of  $\text{CH}_3\text{CHO}$  was detected in the present source sample, it is most likely that  $\text{CH}_3\text{CHO}$  is in fact present in both the warm and cool regions in hot-core sources. The higher rotation temperatures deduced for  $\text{CH}_3\text{OH}$ ,  $\text{C}_2\text{H}_5\text{OH}$ , and  $\text{CH}_3\text{OCH}_3$  indicate that the corresponding emission regions are warmer, denser, and perhaps more compact.

The column densities of  $\text{C}^{17}\text{O}$ , and therefore the deduced column densities of  $\text{H}_2$ , show small variation from source to source, similar to the column densities of the other species. Hence, the inferred molecular abundances are rather constant between the sources. The principal difficulty in deducing fractional abundances with respect to  $\text{H}_2$  is the determination of the corresponding  $\text{H}_2$  column density;  $N(\text{H}_2)$  is usually estimated from  $N(\text{CO})$  which is itself estimated from rarer isotopomers, e.g.  $\text{C}^{18}\text{O}$  or, in our case,  $\text{C}^{17}\text{O}$ . However,  $\text{CO}$  and its isotopomers are, due to their small dipole moments, easily excited in gas of much lower density than are  $c\text{-C}_2\text{H}_4\text{O}$  and  $\text{CH}_3\text{CHO}$ , so the relationship of  $N(\text{CO})$  to  $N(c\text{-C}_2\text{H}_4\text{O})$  is somewhat unclear. We would expect that the fractional abundance relative to  $\text{H}_2$  determined in this way would be a lower limit to the actual value in the denser gas, especially for species whose excitation requirements are much more severe than for  $\text{CO}$ . Column density ratios between e.g.  $c\text{-C}_2\text{H}_4\text{O}$  and  $\text{CH}_3\text{CHO}$  should, however, be more accurate and can be compared between the sources and also to theoretical models (Table 7).

## 5.2. Comparison with chemical models

This survey has shown that ethylene oxide is present in several molecular cloud cores with typical hot-core chemistry, i.e. high abundances of saturated molecules. Ethylene oxide has not, to our knowledge, been explicitly included in any astrochemical models and therefore no comparison with chemical models can be made at present. However, some of the reactions suggested to produce acetaldehyde are probably valid for ethylene oxide as well (cf. Dickens et al. 1997). Therefore, model results obtained for acetaldehyde may, in part, also apply to ethylene oxide.

Standard homogeneous models of gas-phase chemistry do not, in general, reproduce the high abundances of large molecules observed in hot molecular cloud cores. For example, the new standard model by Lee, Bettens, & Herbst (1996) produces a peak fractional abundance of the  $\text{C}_2\text{H}_4\text{O}$  isomers ( $c\text{-C}_2\text{H}_4\text{O}$ ,  $\text{CH}_3\text{CHO}$ , &  $\text{CH}_2\text{CHOH}$ ) of  $9 \times 10^{-12}$  ( $T=10$  K,

$n^3=10^4$   $\text{cm}^{-3}$ , occurring at  $t=10^5$  yr), which is at least a factor of 100 less than the observed abundances reported in the present paper and by Dickens et al. (1997). For  $\text{CH}_3\text{OH}$  and  $\text{CH}_3\text{OCH}_3$ , the predicted abundances are too small by a factor of 30 or more, whereas the predicted abundance of  $\text{HCOOH}$  agrees with observations (peak abundance at  $T=10$  K,  $n=10^4$   $\text{cm}^{-3}$ ,  $t=10^{5.5}$  yr).

To explain the high abundances of saturated molecules, models of hot-core chemistry usually require injection of various molecules from ices, e.g.  $\text{H}_2\text{O}$ ,  $\text{CH}_3\text{OH}$ ,  $\text{NH}_3$ , and  $\text{H}_2\text{CO}$ , into the gas phase at early time to mimic evaporation of grain-mantles. Considering the composition of interstellar ice (e.g. Grim et al. 1991; Schutte et al. 1996), the injection of these species seems very reasonable. The molecules in the model can thus be either (i) pure gas-phase species, for which the grain mantles act merely as storage, (ii) primary dust species, which are formed on grain surfaces and released into the gas phase at the onset of heating, or (iii) secondary dust species, which are formed in the gas phase from dust-evaporated precursor species. The purposes of these time-dependent chemical models are both to constrain the input parameters (input abundances, temperature and density, and the network of chemical reactions) and to predict the evolutionary stage of the modelled source.

Such models have been developed for the hot cores in Orion (Charnley, Tielens, & Millar 1992, hereafter CTM; Caselli, Hasegawa, & Herbst 1993, hereafter CHH) and G34.3+0.2 (Millar, Macdonald, & Gibb 1997, hereafter MMG), which are the best studied objects of this type. In the Orion Compact Ridge, the abundances of  $\text{CH}_3\text{CHO}$ <sup>4</sup>,  $X[\text{CH}_3\text{CHO}] \approx 10^{-9}$  (Turner 1991), and also of  $\text{CH}_3\text{OH}$ ,  $\text{CH}_3\text{OCH}_3$ , and  $\text{HCOOH}$  closely resemble those reported in the present work (Blake et al. 1987), and the chemical models which work for the Compact Ridge therefore work reasonably for the sources reported here as well. None of the oxygen-bearing species have been observed in the Orion Hot Core. The physical conditions in these two hot-core sources are (Blake et al. 1987):  $T_{\text{kin}}=100$  K,  $n=2 \times 10^6$   $\text{cm}^{-3}$  for the Compact Ridge, and  $T_{\text{kin}}=200$  K,  $n=2 \times 10^7$   $\text{cm}^{-3}$  for the Hot Core. Comparing our observed abundances of oxygen-bearing species to the model by CHH we note that the calculated abundances of  $\text{CH}_3\text{OCH}_3$  and  $\text{HCOOH}$  agree with observations. However, the abundances of  $\text{CH}_3\text{OH}$  and  $\text{CH}_3\text{CHO}$  as predicted by the Compact Ridge model are a factor of 5 – 100 too high, whereas the Hot Core model underestimates them by a factor of 100 or more. In the model of the Orion Compact Ridge developed by CTM,  $X[\text{CH}_3\text{OH}]$  and  $X[\text{CH}_3\text{OCH}_3]$  are in agreement with observations, but  $X[\text{CH}_3\text{CHO}]$  is approximately a factor of 10 too low.

The physical and chemical model of G34 by MMG includes contributions to the total column of gas from three components: an ultra-compact core ( $T_{\text{kin}}=300$  K), a compact core ( $T_{\text{kin}}=75$  – 190 K), and an extended halo with decreasing density and temperature. This model reproduces the abundance of  $\text{CH}_3\text{CHO}$  reported here, but overestimates  $X[\text{CH}_3\text{OH}]$  by a factor of 5

<sup>3</sup> Total density of hydrogen nuclei

<sup>4</sup> Using  $N(\text{H}_2)=3 \times 10^{23}$   $\text{cm}^{-2}$  (Blake et al. 1987)

**Table 7.** Observed and theoretical abundance ratios

Source	$\frac{[\text{CH}_3\text{CHO}]}{[\text{c-C}_2\text{H}_4\text{O}]}$	$\frac{[\text{CH}_3\text{OH}]}{[\text{c-C}_2\text{H}_4\text{O}]}$	$\frac{[\text{CH}_3\text{OH}]}{[\text{CH}_3\text{CHO}]}$	$\frac{[\text{CH}_3\text{OH}]}{[\text{CH}_3\text{OCH}_3]}$	Ref.
NGC 6334F	2.6	290	112	9.8	
G327.3–0.6	8.5	320	37	7.4	
G31.41+0.31	2.8	210	78	3.8	
G34.3+0.2	3.9	400	102	7.1	
G10.47+0.03	>5	>660	135	6.2	
TMC-1/L134N	...	...	10	...	MFI, FMHI
Orion Compact Ridge	...	...	70	12	BSMP, T91
Orion Compact Ridge	...	...	1000 <sup>a</sup> /5100 <sup>b</sup>	1500 <sup>a</sup> /50 <sup>b</sup>	CHH/CTM
Orion Hot Core	...	...	8 <sup>c</sup> /5 <sup>d</sup>	510 <sup>c</sup> /1.3×10 <sup>5d</sup>	CHH/CTM
G34.3+0.2	...	...	440 <sup>e</sup>	220 <sup>e</sup>	MMG

MFI: Matthews, Friberg, & Irvine 1985; BSMP: Blake et al. 1987; FMHI: Friberg et al. 1988; CHH: Caselli, Hasegawa, & Herbst 1993; CTM: Charnley, Tielens, & Millar 1992; MMG: Millar, Macdonald, & Gibb 1997; T91: Turner 1991

<sup>a</sup> At  $t=3\times 10^4$  yr

<sup>b</sup> At  $t=4\times 10^4$  yr

<sup>c</sup> At  $t=1\times 10^5$  yr

<sup>d</sup> At  $t=6\times 10^4$  yr

<sup>e</sup> At  $t=10^4/10^5$  yr in the core/halo components

and underestimates  $X[\text{CH}_3\text{OCH}_3]$  by a factor of 10. Most of the modelled column densities of  $\text{CH}_3\text{CHO}$  and  $\text{CH}_3\text{OH}$  arise in the ( $T_{\text{kin}}=300$  K) ultra-compact core. Although the rotation temperatures of  $\text{CH}_3\text{CHO}$  and  $\text{CH}_3\text{OH}$  deduced in this paper, 20 – 80 K, are much lower than 300 K, this is not necessarily in contradiction to theory since the emission from the ultra-compact core is more beam-diluted and hence relatively less significant than the more extended envelope. High-resolution interferometric observations of these molecular lines may be necessary to resolve this issue.

None of these models succeed in fitting the observed abundances of  $\text{CH}_3\text{CHO}$ ,  $\text{CH}_3\text{OH}$ , and  $\text{CH}_3\text{OCH}_3$  simultaneously. The  $[\text{CH}_3\text{OH}]/[\text{CH}_3\text{OCH}_3]$  ratio is far too large in all of the models except that by CTM for the Compact Ridge (Table 7). Unless the observed ratio is systematically underestimated due to a higher beam-filling factor of the  $\text{CH}_3\text{OCH}_3$  emission, this may suggest either that destruction mechanisms for  $\text{CH}_3\text{OH}$  are missing or that  $\text{CH}_3\text{OCH}_3$  is not formed efficiently enough. The  $[\text{CH}_3\text{OH}]/[\text{CH}_3\text{CHO}]$  ratio is also much too high in the models of the Compact Ridge and G34. In the models of the Orion Hot Core, the  $[\text{CH}_3\text{OH}]/[\text{CH}_3\text{CHO}]$  ratio is significantly lower, but none of the species have actually been observed in this source. It is important to bear in mind that the abundances measured in our sources probably are averages over different physical regions, similar to both the Hot Core and Compact Ridge in Orion, because these sources are more distant than Orion.

To our knowledge, no astrochemical models to date succeed in reproducing the observed abundance of ethanol ( $X[\text{C}_2\text{H}_5\text{OH}]\approx 10^{-8}$ ) in conjunction with realistic abundances of other molecules, which may indicate that the pathways to the formation of  $\text{C}_2\text{H}_5\text{OH}$  are poorly understood.

The high abundances of supposedly secondary molecular species, such as  $\text{CH}_3\text{CHO}$  and  $\text{CH}_3\text{OCH}_3$ , obtained in the dif-

ferent hot-core models are rather transient. Usually, significant abundances are only achieved between, roughly,  $10^2 - 10^3$  years to about  $10^5 - 10^6$  years from the onset of dust evaporation. This is consistent with what is known about the lifetime of the ultra-compact H II-regions associated with hot molecular cores (e.g. Churchwell, Walmsley, & Wood 1992, and references therein).

Another interesting point is that both acetaldehyde and methanol have been found to be abundant in the dark clouds TMC-1 and L134 (Matthews, Friberg, & Irvine 1985; Friberg et al. 1988). The  $\text{CH}_3\text{OH}$ -to- $\text{CH}_3\text{CHO}$  ratios are  $\sim 10$  in these sources, compared to  $\sim 100$  in hot cores, thus indicating efficient synthesis of  $\text{CH}_3\text{CHO}$  compared to  $\text{CH}_3\text{OH}$ . Because of the low kinetic temperatures in dark clouds, ice evaporation seems unlikely as a major source of enrichment of the gas. Hence, the hot core models do not seem to provide the full explanation to the observed abundances of these molecules.

## 6. Conclusions

We have detected ethylene oxide ( $\text{c-C}_2\text{H}_4\text{O}$ ) and acetaldehyde ( $\text{CH}_3\text{CHO}$ ) in the hot cores NGC 6334F, G327.3–0.6, G34.3+0.2, and G31.41+0.31. Acetaldehyde was also detected in G10.47+0.03, G322.2+0.6, and Orion 3'N. We also detected lines from  $\text{CH}_3\text{OH}$ ,  $\text{CH}_3\text{OCH}_3$ ,  $\text{C}_2\text{H}_5\text{OH}$ ,  $\text{HCOOH}$ , and  $\text{C}^{17}\text{O}$ . For each of these molecular species, rotation temperatures, column densities and fractional abundances were deduced using a modified rotation diagram analysis. Our main conclusions from these observations are:

- The rotation temperatures are similar for ethylene oxide and acetaldehyde and approximately 20 – 40 K, which indicates that the emission from these molecules originates in the cooler part of the cloud cores. The excitation is probably somewhat subthermal.

- The beam-averaged abundances of ethylene oxide and acetaldehyde are  $(2 - 6) \times 10^{-10}$  and  $(0.8 - 3) \times 10^{-9}$ , respectively. The  $[\text{CH}_3\text{CHO}]/[\text{c-C}_2\text{H}_4\text{O}]$  ratios were found to vary between 2.6 and 8.5.
- The abundances of  $\text{c-C}_2\text{H}_4\text{O}$ ,  $\text{CH}_3\text{CHO}$ ,  $\text{CH}_3\text{OH}$ ,  $\text{CH}_3\text{OCH}_3$ ,  $\text{C}_2\text{H}_5\text{OH}$ , and  $\text{HCOOH}$ , are very similar for NGC 6334F, G327.3–0.6, G34.3+0.2, G31.41+0.31. This suggests that these sources are all in a similar chemical, and possibly evolutionary, state. The abundances of  $\text{CH}_3\text{CHO}$ ,  $\text{CH}_3\text{OH}$ ,  $\text{CH}_3\text{OCH}_3$  and  $\text{HCOOH}$  closely resemble those found in the Orion Compact Ridge.
- To our knowledge, no chemical model can simultaneously reproduce the abundances of all of the large oxygen-bearing molecules observed in these sources.

*Acknowledgements.* AN, PB, and ÅH acknowledge financial support from the Swedish Natural Science Research Council (NFR). JED and WMI were partially supported by NASA grant NAG5-3653. We thank John Black for helpful comments on the manuscript, Luca Olmi for advice on some of the sources, and the SEST staff for help with the observations.

## Appendix A: partition functions and statistical weights

The rotational partition function for an asymmetric rotor without symmetries can be approximated as

$$Q_0(T) \approx \sqrt{\frac{\pi}{ABC}} \left( \frac{kT}{h} \right)^3$$

where  $A$ ,  $B$ , and  $C$  are the rotational constants. For  $\text{c-C}_2\text{H}_4\text{O}$  the partition function becomes

$$Q(T) = \frac{10}{16} \sum_{\text{ortho}} (2J+1) e^{-E_J/kT} + \frac{6}{16} \sum_{\text{para}} (2J+1) e^{-E_J/kT}$$

$$\approx \frac{10}{16} \frac{1}{2} Q_0(T) + \frac{6}{16} \frac{1}{2} Q_0(T) = \frac{1}{2} Q_0(T) \approx 0.945 T^{3/2},$$

which should be used in conjunction with the reduced statistical weights

$$g = \begin{cases} \frac{10}{16} (2J+1) & (ee/oo) \\ \frac{6}{16} (2J+1) & (eo/oe) \end{cases}.$$

The  $\text{CH}_3\text{CHO}$  partition function used is (neglecting the torsional part)

$$Q(T) \approx Q_0^A(T) + Q_0^E(T) \approx 2Q_0(T) \approx 4.60 T^{3/2}$$

and

$$g = 2J + 1.$$

## References

- Batchelor, R. A., Caswell, J. L., Haynes, R. F., Wellington, K. J., Goss, W. M., Knowles, S. H. 1980, *Aust. J. Phys.*, 33, 139
- Bergman, P. 1992, *Modelling of Molecular Clouds*, Technical Report #227, Chalmers University of Technology, Göteborg
- Blake, G. A., Sutton, E. C., Masson, C. R., Phillips, T. G. 1987, *ApJ*, 315, 621
- Caselli, P., Hasegawa, T. I., Herbst, E. 1993, *ApJ*, 408, 548 (CHH)
- Caswell, J. L., Haynes, R. F., Goss, W. M., 1980, *Aust. J. Phys.*, 33, 639
- Cesaroni, R., Walmsley, C. M., Kömpe, C., Churchwell, E. 1991, *A&A*, 252, 278
- Charnley, S. B., Tielens, A. G. G. M., Millar, T. J. 1992, *ApJ*, 399, L71 (CTM)
- Churchwell, E., Walmsley, C. M., Cesaroni, R. 1990, *A&AS*, 83, 119
- Churchwell, E., Walmsley, C. M., Wood, D. O. S. 1992, *A&A*, 253, 541
- Dickens, J. E., Irvine, W. M., Ohishi, M. et al., 1997, *ApJ*, 489, 753
- van Dishoeck, E. F., Blake, G. A. 1998, *ARA&A*, 36, in press
- Frerking, M. A., Langer, W. D., Wilson, R. W. 1982, *ApJ*, 262, 590
- Friberg, P., Madden, S. C., Hjalmarson, Å., Irvine, W. M. 1988, *A&A*, 195, 281
- Gaume, R. A., Fey, A. L., Claussen, M. J. 1994, *ApJ*, 432, 648
- Gaume, R. A., Mutel, R. L. 1987, *ApJS*, 65, 193
- Gezari, D. Y. 1982, *ApJ*, 259, L29
- Gilmore, W., Morris, M., Johnson, D. R. et al., 1976, *ApJ*, 204, 43
- Grim, R. J. A., Baas, F., Greenberg, J. M., Geballe, T. R., Schutte, W. 1991, *A&A*, 243, 473
- Groner, P., Albert, S., Herbst, E., De Lucia, F. C. 1998, *ApJ*, submitted
- Hirose, C. 1974, *ApJ*, 189, L145
- Irvine, W. M., Friberg, P., Kaifu, N. et al., 1989, *ApJ*, 342, 871
- Kleiner, I., Lovas, F. J., Godefroid, M. 1996, *J. Phys. Chem. Ref. Data*, 25, #4, 1113
- Kuiper, T. B. H., Whiteoak, J. B., Fowler, J. W., Rice, W., 1987, *MNRAS*, 227, 1013
- Kutner, M. L., Ulich, B. L. 1981, *ApJ*, 250, 341
- Lampton, M., Margon, B., Bowyer, S. 1976, *ApJ*, 208, 177
- Lee, H.-H., Bettens, R. P. A., Herbst, E. 1996, *A&AS*, 119, 111
- Lovas, F. J., Suenram, R. D., Snyder, L. E., Hollis, J. M., Lees, R. M. 1982, *ApJ*, 253, 149
- Mangum, J. G. 1993, *PASP*, 105, 117
- Matthews, H. E., Friberg, P., Irvine, W. M. 1985, *ApJ*, 290, 609
- Mehring, D. M., Snyder, L. E. 1996, *ApJ*, 471, 897
- Millar, T. J., Macdonald, G. H., Gibb, A. G. 1997, *A&A*, 325, 1163 (MMG)
- Millar, T. J., Macdonald, G. H., Habing, R. J. 1995, *MNRAS*, 273, 25
- Neckel, T. 1978, *A&A*, 69, 51
- Nummelin, A., Bergman, P., Hjalmarson, Å. et al., 1998a, *ApJS*, 117, in press
- Nummelin, A., Bergman, P., Hjalmarson, Å. et al., 1998b, in preparation
- Olmi, L., Cesaroni, R., Walmsley, C. M. 1996, *A&A*, 307, 599
- Pan, J., Albert, S., Sastry, K. V. L. N., Herbst, E., De Lucia, F. C. 1998, *ApJ*, 499, 517
- Pearson, J. C., Sastry, K. V. L. N., Herbst, E., De Lucia, F. C. 1997, *ApJ*, 480, 420
- Penzias, A. A. 1981, *ApJ*, 249, 518
- Shaver, P. A., Goss, W. M. 1970, *Aust. J. Phys. Astrophys. Suppl.*, 14, 77
- Shutte, W. A., Gerakines, P. A., Geballe, T. R., van Dishoeck, E. F., Greenberg, J. M. 1996, *A&A*, 309, 633
- Simpson, J. P., Rubin, R. H. 1990, *ApJ*, 354, 165
- Turner, B. E. 1991, *ApJS*, 76, 617